Electronic reconstruction through the structural and magnetic transitions in detwinned NaFeAs

M Yi[1,2]**, D H Lu**[3]**, R G Moore**[1]**, K Kihou**[4,5]**, C-H Lee**[4,5]**, A Iyo**[4,5]**, H Eisaki**[4,5]**, T Yoshida**[5,6]**, A Fujimori**[5,6]**, Z-X Shen**[1,2]*****

[1]Stanford Institute for Materials and Energy Sciences, SLAC National Accelerator Laboratory, 2575 Sand Hill Road, Menlo Park, California 94025, USA

[2]Geballe Laboratory for Advanced Materials, Departments of Physics and Applied Physics, Stanford University, Stanford, California 94305, USA

[3]Stanford Synchrotron Radiation Lightsource, SLAC National Accelerator Laboratory, 2575 Sand Hill Road, Menlo Park, California 94025, USA

[4]National Institute of Advanced Industrial Science and Technology, Tsukuba, Ibaraki 305-8568, Japan

[5]JST, Transformative Research-Project on Iron Pnictides, Tokyo, 102-0075, Japan

[6]Department of Physics and Department of Complexity Science and Engineering, University of Tokyo, Hongo, Tokyo 113-0033, Japan

*corresponding author: zxshen@stanford.edu

PACS numbers: 74.25.Jb, 74.70.Xa, 79.60.-i

Abstract. We use angle-resolved photoemission spectroscopy to study twinned and detwinned iron pnictide compound NaFeAs. Distinct signatures of electronic reconstruction are observed to occur at the structural (T_S) and magnetic (T_{SDW}) transitions. At T_S, C_4 rotational symmetry is broken in the form of an anisotropic shift of the orthogonal d_{xz} and d_{yz} bands. The magnitude of this orbital anisotropy rapidly develops to near completion upon approaching T_{SDW}, at which temperature band folding occurs via the antiferromagnetic ordering wave vector. Interestingly, the anisotropic band shift onsetting at T_S develops in such a way to enhance the nesting conditions in the C_2 symmetric state, hence is intimately correlated with the long range collinear AFM order. Furthermore, the similar behaviors of the electronic reconstruction in NaFeAs and $Ba(Fe_{1-x}Co_x)_2As_2$ suggests that this rapid development of large orbital anisotropy between T_S and T_{SDW} is likely a general feature of the electronic nematic phase in the iron pnictides, and the associated orbital fluctuations may play an important role in determining the ground state properties.

Electronic reconstruction in detwinned NaFeAs

1. Introduction

Many of the iron pnictide superconductor families share similar phase diagrams in which the underdoped region is marked by two closely-correlated phase transitions: a collinear spin density wave (SDW) transition and a tetragonal to orthorhombic structural transition [1,2]. While the orthorhombic distortion associated with the structural transition breaks the rotational symmetry, the collinear antiferromagnetic (AFM) spin structure formed upon the magnetic transition breaks the translational symmetry. The symmetry-breaking nature of these phases in proximity to high temperature superconductivity in the pnictides makes the study of these competing phases one of high current interest, especially in light of evidences for various broken-symmetries in the pseudogap phase in proximity to superconductivity in the high T_C cuprates [3-5].

Recently, the success of applying uniaxial pressure to detwin pnictide crystals in the orthorhombic phase have led to observations of large in-plane anisotropy in resistivity [6-10] and optical conductivity [11-12]. Surprisingly, the longer and antiferromagnetic direction (x-axis) is found to have smaller resistivity than the shorter and ferromagnetic direction (y-axis). Similar methods also allowed angle-resolved photoemission spectroscopy (ARPES) studies to observe intrinsic broken symmetry of the underlying electronic structure in the SDW state of detwinned $BaFe_2As_2$ [13,14]. Moreover, our previous study on $Ba(Fe_{1-x}Co_x)_2As_2$ (Ba122) revealed that the electronic anisotropy is also manifested in the orbital degree of freedom as an unequal occupation of the d_{xz} and d_{yz} orbitals. This anisotropy onsets near T_S, which occurs above T_{SDW} for x>0, evidencing a non-trivial electronic nematic state in the Ba122 compounds [13].

Up to date, most studies of electronic nematicity in the pnictides have been limited to the 122 compounds. As the magnetic and structural transitions are common features in the phase diagrams of most pnictide families, it is important to establish whether the orbital anisotropy observed in Ba122 is a fundamental phenomenon associated with these competing phases across pnictide families. In this work, we use ARPES to study the evolution of electronic structure through the structural and SDW transitions in NaFeAs, which is the parent compound of a 111 family [15,16]. NaFeAs is an ideal system for ARPES studies due to presence of a charge neutral cleavage plane that minimizes surface problems, as have been reported for both 1111 [17-19] and 122 [20] compounds. Moreover, the large separation of the structural transition (T_S=53K) and SDW transition (T_{SDW}=40K) allows clear identification of the evolution of electronic structure through each transition. Previous ARPES study on twinned NaFeAs [21] reported a rapid shifting of bands onsetting at T_S, which was attributed to band folding due to SDW ordering. In this study, our measurements on detwinned crystals shows that the rapid band shift is actually a symmetry

breaking process in the orbital degree of freedom similar to that observed in Ba122, where the bands of dominant d_{yz} orbital character shift up in the x direction while bands of dominant d_{xz} orbital character shift down in the y direction, breaking the C_4 rotational symmetry. Furthermore, comparison between measurements on detwinned and strain-free twinned crystals shows that this rapid symmetry breaking process onsets near T_S in a strain-free crystal, and the magnitude of orbital anisotropy is almost complete at T_{SDW}, resulting in better nested Fermi surfaces (FS) compared to above T_S. Subsequently, clear signatures of band folding in this symmetry-broken state are observed to onset at T_{SDW}. The clean case of detwinned NaFeAs presented here clarifies the question of how underlying electronic structure evolves through each of the competing phases in iron pnictides as previously complicated by extra surface features in 1111 and 122 as well as those due to domain mixing; and in conjunction with results from 122, also suggests that the electronic nematicity is likely a fundamental phenomenon in underdoped pnictides.

2. Experimental

High quality NaFeAs single crystals were grown by flux method following the recipe described in Kihou *et al* [22], where NaAs was used as a flux. Sample preparation was done in nitrogen glove box to minimize air exposure. ARPES measurements were carried out at beamline 5-4 of the Stanford Synchrotron Radiation Lightsource using a SCIENTA R4000 electron analyzer. ARPES spectra were recorded using 25 eV photons. The total energy resolution was set to 12 meV or better and the angular resolution was 0.3°. Single crystals were cleaved in situ at 10 K for all measurements. All measurements were done in ultra high vacuum chambers with a base pressure better than 4×10^{-11} torr. Crystal detwinning was done similarly as previously reported [13]. Brillouin zone (BZ) notations pertaining to the 2-Fe unit cell is used throughout.

3. Results

3.1. Electronic structure in the paramagnetic state

The observed electronic structure of NaFeAs in the tetragonal state (Fig.1) is similar to other pnictides, with three hole bands near Γ and two electron bands near X. However, one of the hole bands does not appear to cross the Fermi level (E_F), leaving 2 hole pockets and 2 electron pockets on the FS (Fig. 1a), as previously reported [21]. Comparison with LDA calculations [23] shows that an overall renormalization factor of 4 produces a rough match with the overall bandwidths of

measured dispersions near E_F (Fig. 1b), indicating that correlation strength may be stronger in NaFeAs than that in Ba122 [24]. Moreover, a careful look shows that a momentum-dependent shift fine tune is still needed as the LDA bands are higher than measured at Γ, but lower than measured at X, similar to Ba122 [24].

Information of the dominant orbital characters can also be inferred from the analysis of light polarization and orbital symmetries [25], in conjunction with comparison with band structure calculations. According to calculations [26], only the d_{xy}, d_{xz}, and d_{yz} orbitals contribute significantly to the bands near E_F. Along Γ-X in the paramagnetic (PM) state, the α, β, and γ hole bands are predicted to be dominantly d_{xz}, d_{yz}, and d_{xy}, respectively, and the δ and ε electron bands dominantly d_{xz} and d_{xy}. These assignments are consistent with the symmetry constrains in our experiments. Symmetry considerations for the tetragonal state also require d_{xz} and d_{yz} orbitals to be degenerate at the Γ point in the PM state, which appears to be at odds with the assignment of d_{xz} and d_{yz} character to α and β bands. This could be understood by considering the symmetry-allowed hybridization between β and γ bands as they cross each other near Γ and hence open up hybridization gap and switch orbital characters. As a result, the β band with dominant d_{yz} character acquires d_{xy} character approaching Γ while the γ band with dominant d_{xy} character becomes d_{yz} like and is degenerate with the α band (d_{xz}) above E_F at Γ. Such conclusions were also reached in another study [27]. We also note that the d_{xz} electron band (δ) bottom is degenerate with the d_{yz} hole band (β) top at X in the PM state. A summary of the dominant orbital characters of bands near E_F along Γ–X are indicated in Fig. 1c. Those for the Γ–Y direction are by C_4 symmetry derived by an interchange of x and y (*i.e.*, d_{yz} along Γ–X becomes d_{xz} along Γ–Y).

3.2. Electronic structure in the SDW state

Across T_S and T_{SDW} in the low temperature orthorhombic SDW state, significant reconstruction of the electronic structure has occurred, as can be seen from both the FS and band dispersions on twinned NaFeAs (Fig. 1d-f). However, part of the complication comes from domain mixing: the observed dispersions have contribution from both Γ–X direction in one domain and Γ–Y direction in the orthogonal domain. To sort out the intrinsic electronic reconstruction of a single-domain, we measured detwinned crystal.

Figure 2 shows the measured FS and spectral images along Γ–X and Γ–Y of detwinned crystal in the SDW state. The FS near Γ measured in the two geometries do not appear 90° rotated since the polarization used was different with respect to the crystal axes, resulting in different polarization matrix elements that suppress bands of different orbital symmetries in the two

Electronic reconstruction in detwinned NaFeAs

measurements. The fact that they are drastically different demonstrates that the crystal was properly detwinned and that the single-domain electronic structure shows broken rotational symmetry. Note that the high symmetry cut of the twinned crystal (Fig. 1e-f) is indeed a mixture of the Γ–X and Γ–Y cuts (Fig. 2e-f). Comparing these two high symmetry cuts, we see an anisotropy of the bands in a similar fashion as observed on detwinned Ba122, namely that the β band near X is shifted up but shifted down near Y. As this band is dominantly d_{yz} near X and d_{xz} near Y, the offset in energy between these two bands reflects broken rotational symmetry in the orbital degree of freedom. For the electron bands, the shifts are less obvious as their intensity is suppressed by polarization matrix elements. However, the larger k_F opening of the δ electron band along Γ–X in the SDW state seen from remnant intensity (Fig. 2e-f) compared to that in the tetragonal state (Fig. 1c) shows that at least the d_{xz} (δ) electron band along Γ–X is also shifted down. The bottom of the d_{xz} band and the top of the d_{yz} band are no longer degenerate at X as in the tetragonal state. Near Γ, orbital anisotropy can be observed on the γ band near E_F. The k_F of the d_{yz} portion along Γ-X moves away from Γ, signaling shifting up of the d_{yz} hole band, while the opposite happens to the d_{xz} portion along Γ-Y, resulting in an elongation of the outer hole pocket along the Γ-X direction. Similar elongation also happens to the inner hole pocket (Fig. 2c-d), but in the Γ-Y direction to obey the rotated d_{xz}/d_{yz} character. However, we cannot observe whether the degeneracy of the d_{yz} and d_{xz} band tops is lifted at Γ as they remain above E_F. Compared to Ba122 [13], the direction of the orbital anisotropy is the same, namely bands associated with the d_{xz} orbital shift down and bands associated with the d_{yz} orbital shift up.

Besides modification to the electronic structure due to orbital anisotropy, there are also new features indicating band folding as a result of SDW ordering (Fig. 2f). The most pronouncing one is the folding of the γ band, resulting in a hole-like band crossing near X. Likewise the d_{xz} electron band (δ) is also folded from X to Γ (marked by dotted red line in Fig. 2f), as evident in the hybridization gap it opens with the α hole band, which is also mostly d_{xz} character along Γ-X. Folding via (π, π) vector of other bands may also occur, but not observed as clearly in this dataset likely due to intensity suppression by polarization matrix elements.

The crossing of δ band and the folded γ band is especially interesting. The remnant intensity of the crossing points shows the two bands to anti-cross at E_F without opening a gap on the Γ-X high symmetry cut, likely due to their opposite orbital symmetries with respect to Γ-X: d_{xz} for δ and mixed d_{yz}/d_{xy} for γ, resulting in a high intensity spot on the FS. Interestingly, from the FS (Fig. 3a), we observe four such high intensity spots. From the measured band dispersions across each of these spots, we see anti-crossing of bands at E_F (Fig. 3b). This must be the result of the folding of hole bands from Γ and electron bands from X, opening up a hybridization gap

everywhere (Fig. 3 cut2) except at the four high symmetry points in the SDW BZ where hybridization is forbidden by the opposite orbital symmetries of the crossing bands. Two interesting implications should be pointed out. Firstly, anti-crossings on E_F at the extrema points of the FS indicate that the folding pockets are well-nested. Secondly, the separation of the crossings are not the same along Γ-X ($0.42\pi/a$) and Γ-Y ($0.28\pi/b$), indicating that the good nesting is achieved on the elongated hole pockets, which is a direct result of the orbital anisotropy. We also note that the anti-crossings along Γ-X are the protected Dirac nodes predicted by theory [28,29]. This is similar to the case of Ba122 where anti-crossings were also observed in both directions. However, the specific energy positions of the crossings appear material-dependent, as those in $BaFe_2As_2$ cross 30meV below E_F along Γ-Y, indicating varying degree of nesting conditions in different materials depending on the details of the electronic structure.

3.3. Temperature evolution of electronic structure

Next, we examine how these electronic modifications evolve from the PM state to the SDW state through a detailed temperature dependence study. In Fig. 4a-b, we show the spectral images taken on the Y-Γ-X high symmetry lines on a detwinned crystal taken at 10K ($T<T_{SDW}$), 43K ($T_{SDW}<T<T_S$), and 70K ($T_S<T$), together with the β and δ band dispersions derived from the tetragonal PM state for comparison. Qualitatively, we see that on one hand, the anisotropic shifts in the β and δ bands along the two directions clearly persist above T_{SDW}, and diminish above T_S. On the other hand, the signatures of SDW folding—γ hole band folding and anti-crossing with the δ band near X and the hybridization gap of the folded δ band (d_{xz}) with the α hole band (d_{xz})—are clearly observed for $T< T_{SDW}$, but disappears just above T_{SDW}. The temperature dependence of these electronic evolutions can be further visualized quantitatively. First, we look at the β band shifts near X/Y, and measure its shifting energy position as a function of temperature. This can be done directly for the strain-free twinned crystal as the β band from both Γ-X and Γ-Y directions appear on the same cut due to domain mixing (Fig. 4c-d). The energy positions of the β band from the two directions can be determined simultaneously from the corresponding peaks in the energy distribution curve (EDC) on twinned crystal. We plot the EDC for a representative momentum position A at each temperature, where the peaks marked by red/green diamonds are the β bands from Γ-Y and Γ-X directions, respectively (Fig. 4e). In addition, a third peak near E_F appears due to γ band folding, which will be discussed later. The positions of these peaks can be better determined from the second derivatives of the EDCs, where the band positions show up as dips (Fig. 4f). From the temperature dependence of the energy positions of these two bands (Fig.

4g), we see that they are degenerate in energy above T_S, as expected under C_4 symmetry in the tetragonal state. Near T_S, they begin to separate in energy, signaling the onset of orbital anisotropy already at the structural transition. It is interesting to note that the energy separation already reaches near completion by T_{SDW}, below which minimal change is observed. The full energy separation is on the order of 30meV in NaFeAs, compared to 60meV in $BaFe_2As_2$, which has both bigger magnetic moment ($0.8\mu_B$ [30] compared to $0.3\mu_B$ for NaFeAs [31]) and higher transition temperatures ($T_S = T_{SDW} = 140K$). The same temperature dependent measurements can be done on the orthogonal directions on detwinned crystals, which are plotted in Fig. 4g for comparison. The major difference is that the anisotropy on detwinned crystals onsets far above T_S (defined for unstressed crystals), similar to the observation in detwinned Ba122. This is consistent with detwinning pressure dependent resistivity measurement [6] showing smearing of T_S due to the symmetry-breaking field of the uniaxial strain, suggesting a large nematic susceptibility and strong orbital fluctuations associated with T_S as revealed by the detwinning stress.

Next, we look at the signatures of band folding by examining the temperature dependence of the folded γ hole band near X from both EDC and MDC. On the EDC, as seen from twinned sample (Fig. 4e), the peak closest to E_F (marked in blue) corresponding to the folded γ band only appears below T_{SDW}. The behavior is even clearer on the MDC taken slightly below E_F on detwinned crystal (Fig. 4h). Two peaks are observed there, corresponding to the folded γ band on the left and the original δ electron band on the right. The feature corresponding to the folded γ band only appears below T_{SDW}.

To summarize the temperature evolution of electronic reconstruction (Fig. 5), we observe distinct electronic reconstruction onsetting at T_S and T_{SDW}. For strain-free twinned crystals, rotational symmetry breaking modification to the electronic structure begins near T_S as orbital anisotropy onsets, manifested in the upward shifting of d_{yz} bands and downward shifting of d_{xz} bands. Such anisotropy develops towards T_{SDW}, at which temperature long range magnetic ordering sets in and band folding occurs on top of the anisotropic electronic structure due to the broken translational symmetry, resulting in smaller reconstructed FS pockets. From the experimental point of view, measurement on detwinned crystal is crucial for disentangling the electronic reconstruction and symmetry breaking process through each transition.

4. Discussion

One of the current focuses in the pnictide community is to understand the dominating mechanisms responsible for the pervasive structural and magnetic transitions in the phase

diagram and their connection to the emerging superconductivity. Many theoretical proposals have been put forth in this regard, especially in light of many recent experimental findings of the large electronic nematicity associated with the structural transition. Such theoretical endeavors include those driven by magnetism [32-37], in which a symmetry-breaking Ising nematic phase can emerge above T_{SDW} via spin fluctuations; those based on orbital ordering [38-44] reflected in symmetry breaking via an unequal occupation of the d_{yz} and d_{xz} orbitals onsetting at the higher symmetry-breaking phase transition of T_S; those based on a Pomeranchuk instability between the near nesting of the C_4 symmetric d_{xy} hole pocket and the elliptical electron pockets [45]; and symmetry breaking from a valley-density wave and hidden orders [46]. Experimental understanding of what occurs at these two transitions is important to distinguish amongst these proposals.

Here in this work, the observed sequential development of orbital anisotropy at the higher T_S and then band folding at the lower T_{SDW} reveals an interesting connection between these two transitions. As we have noted, the electron and hole bands that fold appear to have good nesting condition. However, such nesting is observed to be achieved at T_{SDW} *after* the full development of anisotropic band shift between T_S and T_{SDW}, evident in the elongated shape of the folding hole pockets. One natural interpretation of this observation is that at T_S, orbital anisotropy begins to develop, breaking the C_4 rotational symmetry of the FS and lifting the degeneracy of the nesting instabilities between Γ-X and Γ-Y as one is enhanced and the other suppressed. At T_{SDW}, the nesting instability of the favored direction diverges and drives the collinear AFM order as the bands fold in this direction. Such a scenario was also proposed by Kontani *et al.* based on the orbital fluctuation theory [47]. This sequence of electronic evolution also explains the observed onset of an enhancement of spin fluctuations at T_S and its divergence towards T_{SDW} in NMR measurements of NaFeAs [31].

In a bigger context, we see that the case of NaFeAs and that of Ba122 [13] are very similar: i) the anisotropic orbital/band shift is always associated with the rotational symmetry breaking at T_S; ii) the direction of orbital anisotropy is the same with d_{xz} (d_{yz}) bands shifting down (up). The well-separated transitions and lack of surface complications in NaFeAs here allowed us to see more clearly what occurs at T_{SDW}. Such an orbital anisotropy-enhanced nesting-driven AFM order implies that the underlying electronic structure with its orbital content plays a governing role for these two transitions. While the large orbital anisotropy of the nematic phase may be a general phenomenon for iron pnictides that share similar electronic structure, the subtle difference in the electronic structure may be held accountable for the variation of the relation between these two transitions from family to family or with doping, as to be understood with

Electronic reconstruction in detwinned NaFeAs

further work. Nonetheless, our observation reveals a strong coupling of the orbital fluctuations associated with the onset of orbital anisotropy at T_S and the enhanced spin fluctuations in the electronic nematic phase. And the consideration of the interplay between these two fluctuations may be critical in understanding the emerging superconducting phase in the pnictides.

Note: After the submission of this paper, a work of smiliar nature on detwinned NaFeAs appeared, in which the authors reported similar results as reported here[48].

Acknowledgements

Electronic reconstruction in detwinned NaFeAs

References

1. Paglione J P and Greene R L 2010 High-temperature superconductivity in iron-based materials *Nature Physics* **6** 645

2. Johnston D C 2010 The Puzzle of High Temperature Superconductivity in Layered Iron Pnictides and Chalcogenides *Advances in Physics* **59** 803-1061

3. Daou R *et al* 2010 Broken rotational symmetry in the pseudogap phase of a high-T_C superconductor *Nature* **463** 519

4. Lawler M J *et al* 2010 Intra-unit-cell electronic nematicity of the high-T_C copper-oxide pseudogap states *Nature* **466** 347

5. Hashimoto M *et al* 2010 Particle-hole symmetry breaking in the pseudogap state of Bi2201 *Nature Physics* **6** 414

6. Chu J-H *et al* 2010 In-Plane Resistivity Anisotropy in an Underdoped Iron Arsenide Superconductor *Science* **329** 824

7. Tanatar M A *et al* 2010 Uniaxial-strain mechanical detwinning of $CaFe_2As_2$ and $BaFe_2As_2$ crystals: Optical and transport study *Phys. Rev. B* **81** 184508

8. Ying J J *et al* 2011 Measurements of the Anisotropic In-Plane Resistivity of Underdoped FeAs-Based Pnictide Superconductors *Phys. Rev. Lett.* **107** 067001

9. Blomberg E C *et al* 2011 In-plane anisotropy of electrical resistivity in strain-detwinned $SrFe_2As_2$ *Phys. Rev. B* **83** 134505

10. Fisher I R, Degiorgi L and Shen Z-X 2011 In-plane electronic anisotropy of underdoped "122" Fe-arsenide superconductors revealed by measurements of detwinned single crystals *Rep. Prog. Phys.* **74** 124506

11. Dusza A *et al* 2011 Anisotropic charge dynamics in detwinned $Ba(Fe_{1-x}Co_x)_2As_2$ *Europhys. Lett.* **93** 37002

12. Nakajima M *et al* 2011 Unprecedented anisotropic metallic state in $BaFe_2As_2$ revealed by optical spectroscopy *PNAS* **108** (30) 12238-12242

13. Yi M *et al* 2011 Symmetry breaking orbital anisotropy observed for detwinned $Ba(Fe_{1-x}Co_x)_2As_2$ above the spin density wave transition *PNAS* **108** (17) 6878

14. Kim Y K *et al* 2011 Electronic structure of detwinned $BaFe_2As_2$ from photoemission and first principles *Phys. Rev. B* **83** 064509

15. Chen G F, Hu W Z, Luo J L and Wang N L 2009 Multiple Phase Transitions in Single-Crystalline $Na_{1-\delta}FeAs$ *Phys. Rev. Lett.* **102** 227004

16. Parker D R *et al* 2010 Control of the Competition between a magnetic phase and a superconducting phase in cobalt-doped and Nickel-Doped NaFeAs Using Electron Count *Phys. Rev. Lett.* **104** 057007

17. Lu D H *et al* 2008 Electronic structure of the iron-based superconductor LaOFeP *Nature* **455** 81

18. Yang L X *et al* 2010 Surface and bulk electronic structures of LaOFeAs studied by angle resolved photoemission spectroscopy *Phys. Rev. B* **82** 104519

19. Liu C *et al* 2010 Surface-driven electronic structure in LaFeAsO studied by angle-resolved photoemission spectroscopy *Phys. Rev. B* **82** 075135

20. Jensen M F *et al* 2011 Angle-resolved photoemission study of the role of nesting and orbital orderings in the antiferromagnetic phase of $BaFe_2As_2$ arXiv: 1105.5605

21. He C *et al* 2010 Electronic-Sturcture-Driven Magnetic and Structure Transitions in Superconducting NaFeAs Single Crystals Measured by Angle-Resolved Photoemission Spectroscopy *Phys. Rev. Lett.* **105** 117002

22. Kihou K *et al* 2010 Single Crystal Growth and Characterization of the Iron-Based Superconductor KFe2As2 Synthesized by KAs Flux Method *J. Phys. Soc. Jpn.* **79** 124713

23. Deng S, Kohler J and Simon A 2009 Electronic structure and lattice dynamics of NaFeAs *Phys. Rev. B* **80** 214508

24. Yi M *et al* 2009 Electronic structure of the $BaFe_2As_2$ family of iron-pnictide superconductors *Phys. Rev. B* **80** 024515

25. Damascelli A, Hussain Z and Shen Z-X 2003 Angle-resolved photoemission studies of the cuprate superconductors *Rev. Mod. Phys.* **75** 473

26. Graser S *et al* 2010 Spin fluctuation sand superconductivity in a three-dimensional tight-binding model for $BaFe_2As_2$ *Phys Rev B* **81** 214503

27. He C *et al* 2010 The orbital characters and k_z dispersions of bands in iron-pnictide NaFeAs *Journal of Physics and Chemistry of Solids* **72** 479

28. Ran Y *et al* 2009 Nodal spin density wave and band topology of the FeAs-based materials *Phys. Rev. B* **79** 014505

29. Morinari T Kaneshita E Tohyama T 2010 Topological and Transport Properties of Dirac Fermions in an Antiferromagnetic Metallic Phase of Iron-Based Superconductors *Phys. Rev. Lett.* **105** 037203

30. Huang Q *et al* 2008 Neutron-Diffraction Measurements of Magnetic Order and a Structural Transition in the Parent $BaFe_2As_2$ Compound of FeAs-Based High-Temperature Superconductors *Phys. Rev. Lett.* **101** 257003

31. Ma L *et al* 2011 ^{23}Na and ^{75}As NMR study of antiferromagnetism and spin fluctuations in NaFeAs single crystals *Phys. Rev. B* **83** 132501

32. Mazin I I and Johannes M D 2009 A key role for unusual spin dynamics in ferropnictides *Nature Physics* **5** 141

33. Fang C *et al* 2008 Theory of electron nematic order in LaFeAsO *Phys. Rev. B* **77** 224509

34. Xu C Muller M Sachdev S 2008 Ising and spin orders in the iron-based superconductors *Phys. Rev. B* **78** 020501(R)

35. Fernandes R *et al* 2009 Effects of Nematic fluctuations on the elastic properties of iron-arsenide superconductors *Phys. Rev. Lett.* **105** 157003

36. Fernandes R *et al* 2012 Preemptive nematic order, pseudogap, and orbital order in the iron pnictides *Phys. Rev. B* **85** 024534

37. Daghofer M Nicholson A Moreo A and Dagotto E 2010 Three orbital model for the iron-based superconductors *Phys. Rev. B* **81** 014511

38. Lee C-C, Yin W-G and Ku W 2009 Ferro-Orbital Order and Strong Magnetic Anisotropy in the Parent Compounds of Iron-Pnictide Superconductors *Phys. Rev. Lett*. **103** 267001

39. Kruger F, Kumar S, Zaanen J and van den Brink J 2009 Spin-orbital frustrations and anomalous metallic state in iron-pnictide superconductors *Phys. Rev. B* **79** 054504

40. Bascones E, Calderon MJ and Valenzuela B 2010 Low Magnetization and Anisotropy in the Antiferromagnetic State of Undoped Iron Pnictides *Phys. Rev. Lett.* **104** 227201

41. Yin Z P and Pickett W E 2010 Crystal symmetry and magnetic order in iron pnictides: A tight-binding Wannier function analysis *Phys. Rev. B* **81** 174534

42. Lv W, Kruger F and Phillips P 2010 Orbital Ordering and Unfrustrated $(\pi,0)$ Magnetism from Degenerate Double Exchange in the Pnictides *Phys. Rev. B* **82** 045125

43. Chen C-C *et al* 2010 Orbital Order and Spontaneous Orthorhombicity in Iron pnictides *Phys. Rev. B* **82** 100504(R)

44. Laad M S and Craco L 2010 Theory of Orbital Nematicity in Underdoped Iron Arsenides arXiv 1010.2940

45. Zhai H, Wang F and Lee D-H 2009 Antiferromagnetically driven electronic correlations in iron pnictides and cuprates *Phys. Rev. B* **80** 064517

46. Kang J and Tesanovic Z 2011 Theory of the valley-density wave and hidden order in iron pnictides *Phys. Rev. B* **83** 020505

47. Kontani H, Saito T and Onari S 2011 Origin of Orthorhombic Transition, Magnetic Transition, and Shear Modulus Softening in Iron Pnictide Superconductors: Analysis based on the Orbital Fluctuation Theory *Phys. Rev. B* **84** 024528

48. Zhang Y *et al* 2012 Symmetry breaking via orbital-dependent reconstruction of electronic structure in detwinned NaFeAs *Phys. Rev. B* **85** 085121

Electronic reconstruction in detwinned NaFeAs
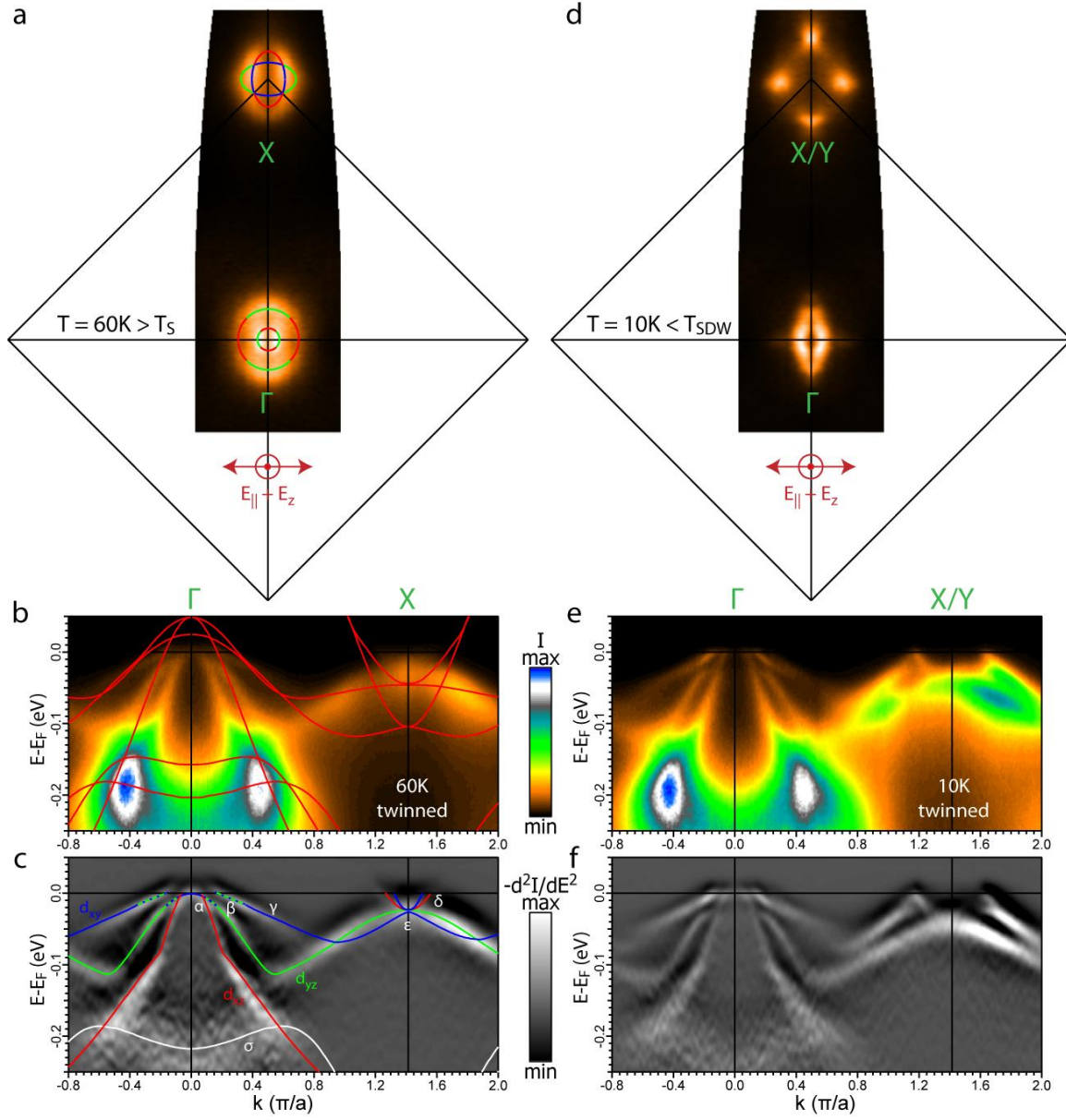
Figure 1

Electronic structure of twinned NaFeAs. (a) FS measured in the tetragonal PM state at 60K. (b) Spectral image along the Γ-X high symmetry cut, overlaid with LDA calculations which were renormalized by a factor of 4. (c) Second derivative of (b), overlaid with band guides to eye marked with dominant orbital contribution (red/ green/blue: $d_{xz}/d_{yz}/d_{xy}$). Dotted colors denote mixed orbital characters (see text). (d)-(f) Same as that of (a)-(c) but taken in the SDW state at 10K. The FS were symmetrized according to crystal symmetry.
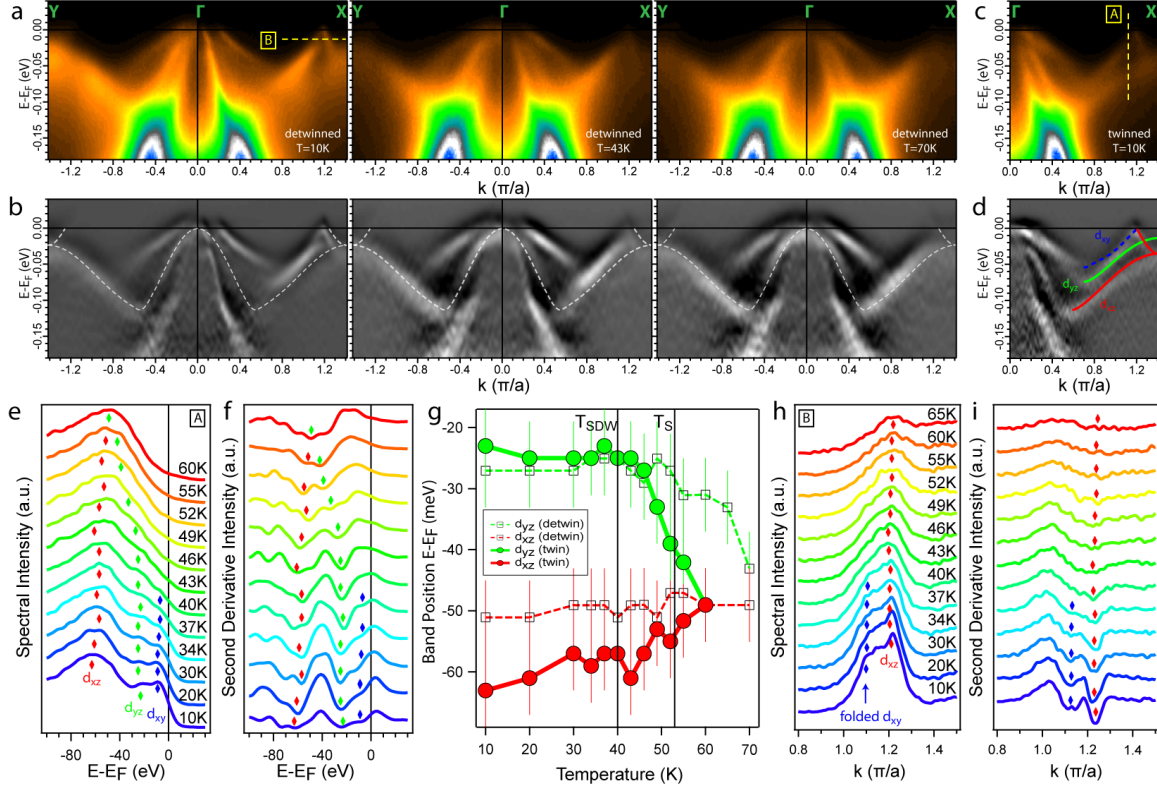
Electronic reconstruction in detwinned NaFeAs
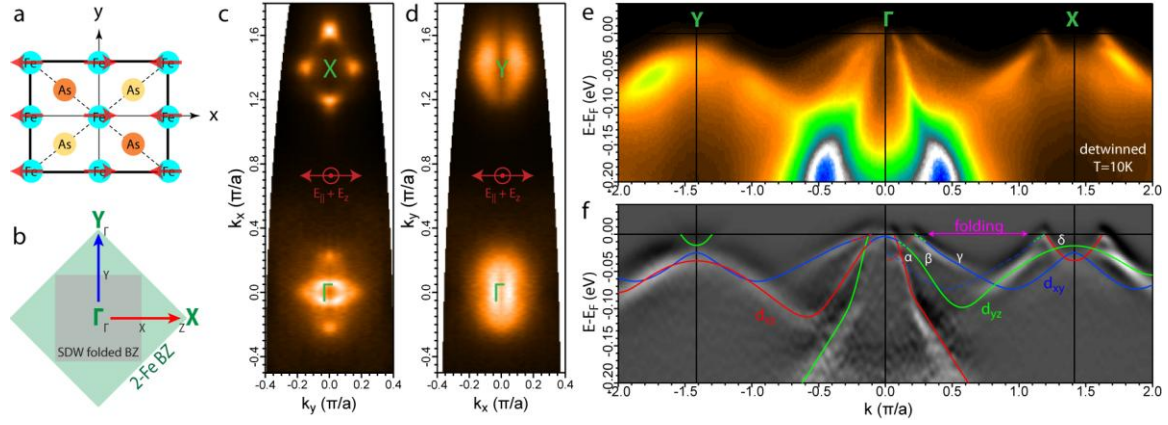
Figure 2

Electronic anisotropy observed in the SDW state of detwinned NaFeAs. (a) Schematic of orthorhombic SDW unit cell. (b) BZ definitions for the tetragonal PM state (green) and orthorhombic SDW state (gray). PM BZ (green) notations are used throughout, where Γ-X (Γ-Y) is along the AFM (FM) direction. (c)-(d) FS measured along Γ-X and Γ-Y directions, respectively, with polarization vectors labeled in red. (e) Spectral image along Y-Γ-X high symmetry directions. (f) Second derivative image of (e). Band eye guides for prominent observable bands are marked with dominant orbital characters. Weaker dotted lines denote folded bands. All data were measured at 10K on detwinned crystal.

Electronic reconstruction in detwinned NaFeAs
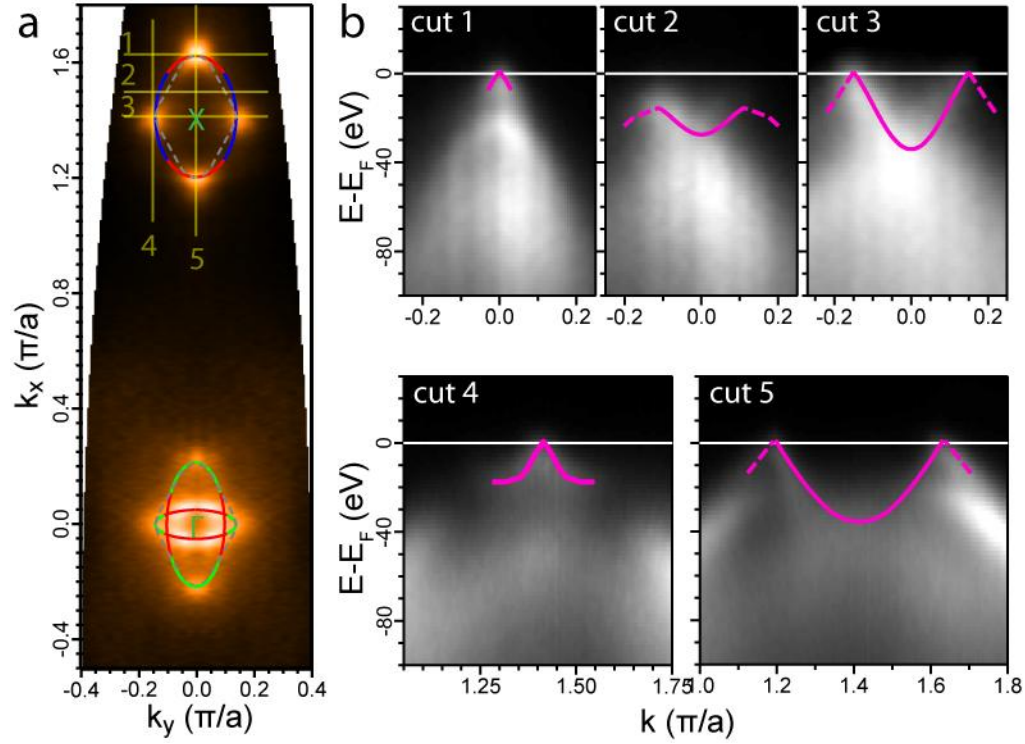
Figure 3

Band crossings of folded hole and electron bands in the SDW state. (a) FS measured along Γ-X on detwinned crystal, where the folding hole pockets at Γ (blue) and electron pocket at X are marked. Dotted contour mark where hybridization gap is opened. (b) Spectral images along various cuts marked in (a), where zero gap is observed at the high symmetry points of folded bands, and finite hybridization gap is observed elsewhere. Measurements taken at 10K.

Electronic reconstruction in detwinned NaFeAs

Figure 4

Temperature evolution of the electronic reconstruction. (a)-(b) Spectral image and its second derivative along Γ-X/Y high symmetry direction measured at 10K on twinned crystal. (c)-(d) Spectral image and its second derivative along Y-Γ-X high symmetry cuts on detwinned crystal at 10K (T<T_{SDW}), 43K (T_{SDW}<T<T_S), and 70K (T_S<T). Dotted lines mark the β band position in the PM state for comparison. (e) Temperature evolution of the EDC cut labeled as A in (a), where peak positions are marked to indicate band positions. (f) Second derivatives of the EDCs in (e), where dips indicate band positions. (g) Temperature dependence of the d_{yz} (green) and d_{xz} (red) band positions measured at momentum A on twinned and detwinned crystals. (h) Temperature evolution of the MDC cut labeled as B in (c). (i) Second derivatives for the MDCs in (h).

Electronic reconstruction in detwinned NaFeAs
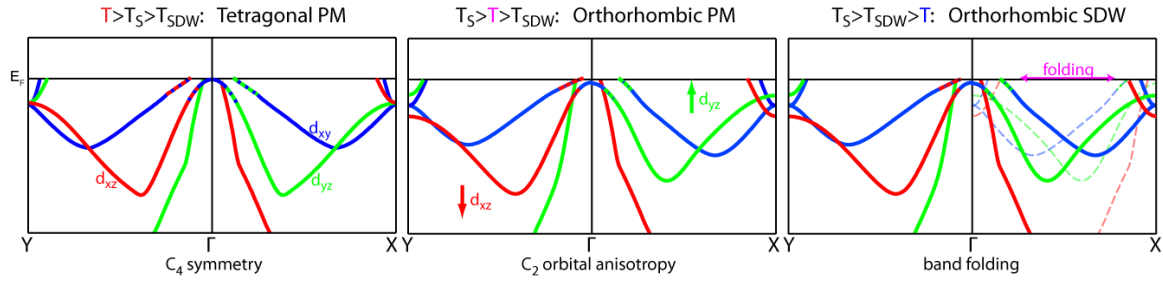
Figure 5

Schematic of electronic structure evolution. In the tetragonal PM state, the electronic structure is C_4 symmetric. As temperature is cooled upon T_S, C_4 symmetry is broken as bands of dominant d_{xz} character shift down and bands of dominant d_{yz} character shift up. Upon further cooling, at T_{SDW}, band folding occurs along the AFM direction (Γ-X), and hybridization gaps may open where allowed by orbital symmetry (not shown).